
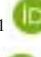




Solar magnetic activity and its terrestrial impact through correlations with drought indices

A. Sarsembayeva^{1*} , L. Ryssaliyeva¹ ,
F. Belissarova¹  and A. Sarsembay² 

¹Al-Farabi Kazakh National University, Almaty, Kazakhstan

²CSI «Kyzylorda Regional Educational Center (Methodological Office)»
of the Department of Education of Kyzylorda Region, Kyzylorda, Kazakhstan

*e-mail: sarsembayeva.a@kaznu.kz

(Received April 5, 2025; received in revised form May 17, 2025; accepted May 26, 2025)

Solar activity manifests itself in the form of sunspots on the solar surface and solar flares, which can influence Earth's climatic conditions, including drought in mid-latitude regions. This study examines the impact of solar flares on drought conditions in Northern Kazakhstan and analyzes the relationship between solar activity parameters and drought indices. Twelve solar flares of classes X and M recorded in 2014 were analyzed using multi-wavelength data from SDO/AIA, GOES, and HMI/SOLIS magnetograms. Key physical parameters of the flares were determined, including duration, spatial scale, and magnetic reconnection rate. The reconnection rates ranged from 10^{-4} to 10^{-3} and showed an inverse dependence on the GOES classification, consistent with the Petschek reconnection theory. Additionally, correlation links were investigated between solar activity indices (WSN, SSN), atmospheric oscillations (NAO, AO), and drought indices (SPI3, HTC). Significant strong correlations were established: between WSN and NAO ($r = 0.63$), NAO and SPI3 ($r = 0.70$), as well as a strong negative correlation between SSN and HTC ($r = -0.66$), indicating a potential connection between solar activity and drought formation in temperate regions.

Key words: solar flares, magnetic reconnection, sunspot activity, drought indices, atmospheric oscillations.

PACS number(s): 96.60.-j; 96.60.Iv; 96.60.qe.

1 Introduction

Solar activity plays a crucial role in driving dynamic processes within the solar atmosphere and throughout the heliosphere, exerting measurable influence on the Earth's magnetosphere, ionosphere, and atmospheric systems [1]. Among the most energetic manifestations of solar activity are solar flares – sudden, intense releases of energy across the entire electromagnetic spectrum. These events are accompanied by bursts of X-rays, ultraviolet radiation, and radio waves, reflecting the rapid acceleration of charged particles and the presence of high-temperature plasma. The primary mechanism responsible for such rapid energy release is magnetic reconnection, which occurs in regions of strongly sheared or oppositely directed magnetic fields in the solar corona [2-3].

Solar flares are well known for their impact on space weather conditions, including transient increases in high-energy particle fluxes, cosmic ray modulation, and the intensification of the solar

wind. These phenomena lead to compression of the Earth's magnetosphere, often resulting in geomagnetic storms with an observed delay of approximately 36 hours after the flare event. Observational data from missions such as SOHO, STEREO, and the Solar Dynamics Observatory (SDO) have enabled high-resolution, multi-wavelength imaging of these events, allowing detailed reconstruction of their physical parameters. Nevertheless, the volume and cadence of full-disk, high-temporal-resolution imagery present computational challenges for data access and processing [4].

In this study, we analyze 12 major X- and M-class solar flares recorded between January 2014 and December 2024, employing multi-wavelength imaging from AIA/SDO and magnetograms from HMI, SOLIS, and GOES. We estimate key physical properties of these flares – including duration, spatial scale, magnetic flux density, and reconnection rate – to characterize the flare energetics and reconnection dynamics. Our results

reveal notable trends, including a broader size distribution for weaker GOES classes, a lower threshold in magnetic flux density that depends on flare class, and a decreasing reconnection rate with increasing flare magnitude. Calculated inflow velocities range from a few to several tens of kilometers per second, while estimated coronal Alfvén velocity fall within the 10^3 – 10^4 km/s range, yielding dimensionless reconnection rates on the order of 10^{-3} – consistent with theoretical predictions from fast reconnection models.

Beyond the immediate impacts on the near-Earth environment, long-term solar variability, as indexed by sunspot numbers such as SSN, WSN, and GSN, is increasingly recognized as a potential driver of terrestrial climate modulation. These indices follow an approximate 11-year solar cycle [5-6] and have been statistically associated with cyclic variations in surface temperature, precipitation, and large-scale atmospheric oscillations. Although the overall variation in total solar irradiance is small ($\sim 0.04\%$), the resulting changes in upper atmospheric dynamics – particularly through enhanced UV radiation and stratospheric heating – can significantly influence tropospheric circulation patterns. Empirical studies have linked solar activity to modulations in the El Niño–Southern Oscillation (ENSO), Arctic Oscillation (AO), and North Atlantic Oscillation (NAO), which serve as critical regulators of climate variability, particularly in the Northern Hemisphere [7-9].

However, the climatic response to solar forcing is region-dependent and often non-linear. In West Africa, for instance, positive correlations between solar activity and both temperature and precipitation have been reported, particularly during solar minima, often resulting in intensified heat extremes [10-11]. Similarly, studies in India have identified links between solar cycles and monsoonal variability [12-13]. In contrast, regions such as East Africa, the United States, and Saudi Arabia show weaker or statistically insignificant correlations [14-15], potentially due to hemispheric asymmetry in sunspot distribution and flare emergence [16].

Given these complexities, the current study takes an interdisciplinary approach, bridging solar physics and atmospheric science to investigate the impact of solar magnetic activity and flare energy release on regional drought conditions. Specifically, we explore how flare-scale parameters – such as reconnection rate and spatial scale – correlate with

climate indicators including the Standardized Precipitation Index (SPI3) and the Selyaninov Hydrothermal Coefficient (HTC), using data from Northern Kazakhstan, a region highly vulnerable to agricultural drought. We further examine the role of atmospheric teleconnections such as NAO and AO, which may act as intermediaries in the solar–climate interaction.

2 Data analysis

The energy released during a solar flare can be attributed to the magnetic energy stored in the solar corona, which is generally expressed as a function of the flare’s characteristic spatial scale and the magnetic flux density present in the active region [17].

$$E_{flare} \sim E_{mag} = \frac{B_{cor}^2}{8\pi} L^3 \quad (1)$$

Since the liberated magnetic energy corresponds to the energy transported into the magnetic reconnection region, the rate of energy release can be formulated based on the inflow velocity of plasma into this region [18-20].

$$\left| \frac{dE_{mag}}{dt} \right| \sim 2 \frac{B_{cor}^2}{4\pi} V_{in} L^2 \quad (2)$$

Accordingly, the duration required for this inflow to supply the total energy released by the flare provides an estimate of the flare’s characteristic timescale.

$$\tau_{flare} \sim E_{flare} \left(\left| \frac{dE_{mag}}{dt} \right| \right)^{-1} \sim \frac{L}{4V_{in}} \quad (3)$$

This relationship allows for the determination of the plasma inflow velocity using observationally derived timescale values.

$$V_{in} \sim \frac{L}{4\tau_{flare}} \quad (4)$$

To assess the reconnection process $M_A \equiv \frac{V_{in}}{V_A}$, in a dimensionless framework, we must estimate the Alfvén velocity $V_A = \frac{B_{cor}}{(4\pi\rho)^{1/2}}$ in the inflow region, which depends on the coronal magnetic field strength and plasma density. Therefore, by measuring the coronal density B_{cor} , flare size L ,

magnetic field strength, and flare duration τ_{flare} , it becomes possible to compute key physical parameters: the plasma inflow velocity V_{in} , the Alfvén velocity V_A , and the corresponding magnetic reconnection rate M_A [21-22].

Observational data for this analysis is provided in near real-time by the Geostationary Operational Environmental Satellites (GOES), which monitor solar flares and associated energetic particles. In particular, data from GOES-13, GOES-14, and GOES-15 were used to track X-ray flux variations during flare events.

Beyond solar flare diagnostics, this study also investigates the climatic impact of solar activity on regional drought in Northern Kazakhstan – a region of significant agricultural importance and sensitivity to climate variability. In particular, drought events pose a major threat to wheat production, with losses reaching up to 50% in dry years and leading to substantial economic damage.

Meteorological data for the year 2014 were obtained from the Republican State Enterprise "Kazhydromet", under the Ministry of Ecology and Natural Resources. These data include monthly total precipitation and daily mean air temperature from 11 ground-based weather stations across the North Kazakhstan region. Based on these inputs, two drought indices were computed: the Standardized Precipitation Index (SPI) and the Selyaninov Hydrothermal Coefficient (HTC).

The SPI is a globally recognized index recommended by the World Meteorological Organization (WMO). It is based solely on precipitation and is suitable for assessing drought over various time scales. SPI is calculated by fitting precipitation data to a gamma distribution, which is then transformed into a normal distribution. Positive SPI values indicate wetter-than-average conditions, while negative values reflect meteorological drought [23].

The Selyaninov Hydrothermal Coefficient (HTC) is commonly used in agricultural climatology to assess moisture availability. It is defined as:

$$HTC = \frac{\sum R}{0.1 \sum t} \quad (5)$$

where: t is the sum of average daily air temperatures during the period when air temperatures are above +10 °C, and R is the total precipitation during the same period, in mm [24].

Additionally, the North Atlantic Oscillation (NAO) and Arctic Oscillation (AO) indices were incorporated to assess atmospheric circulation influences. NAO data were retrieved from the National Centers for Environmental Information (NCEI) under NOAA, while AO data were obtained from the Physical Sciences Laboratory (PSL) of NOAA's Earth System Research Laboratories [25-26].

By integrating solar flare diagnostics with regional drought indices and large-scale atmospheric oscillation data, we aim to quantify the extent to which solar magnetic activity and flare dynamics may influence terrestrial climate variability and drought risk across continental mid-latitudes.

3 Results

This study integrates solar flare diagnostics with atmospheric circulation and drought indices to investigate the potential solar-terrestrial coupling mechanisms influencing regional hydrometeorological variability in Northern Kazakhstan. We present results from two complementary domains: (1) the physical characterization of solar flares based on reconnection dynamics and flare morphology, and (2) the statistical correlation between solar activity indices and atmospheric/drought indicators throughout the year 2014.

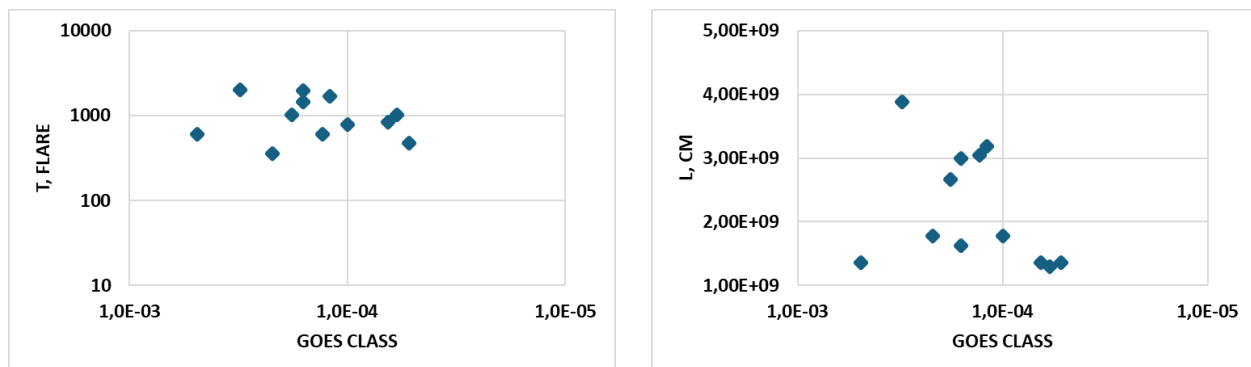


Figure 1 – Physical parameters of each flare plotted against the GOES class (a); Timescale T_{flare} . Size L (b)

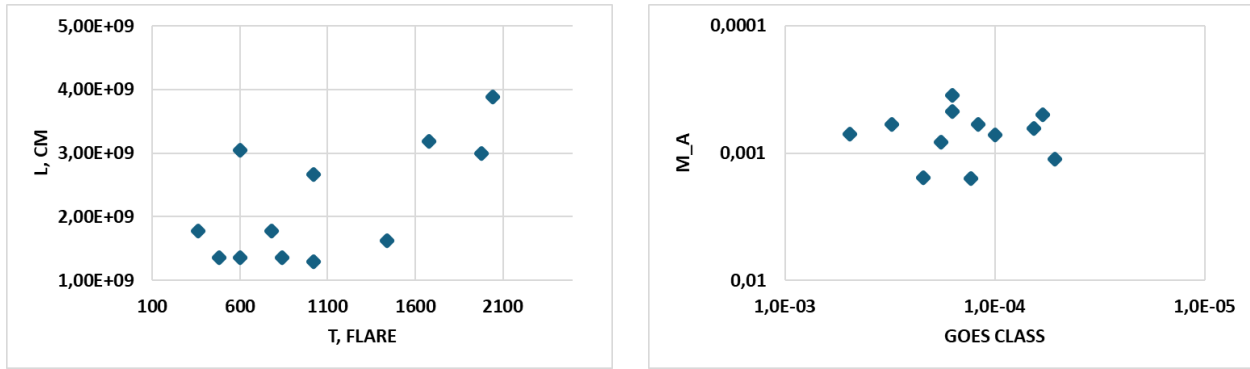


Figure 2 – Timescale τ_{flare} plotted against L (a); Reconnection rate M_A plotted against GOES class (b)

3.1. Physical parameters of solar flares

In this study, we analyzed 12 major X- and M-class solar flares observed during the year 2014 to investigate the physical parameters governing energy release through magnetic reconnection. Using multi-wavelength observations and magnetogram data, we derived flare timescales (τ_{flare}), characteristic sizes (L), reconnection rates (M_A), and compared these parameters with GOES peak X-ray flux to explore physical trends and potential scaling relations.

3.1.1 Flare duration vs. GOES class

Fig. 1a displays the relationship between the flare timescale (τ_{flare}) and the GOES class on a log-log scale. The flare durations range from approximately 500 to 2000 seconds. The scatter plot shows a weak inverse trend, suggesting that higher GOES-class flares tend to have slightly shorter durations, while weaker flares exhibit a broader range of timescales (Fig. 1a).

3.1.2 Flare size vs. GOES class

In Fig. 1b, the characteristic spatial size of the flare loops (L) is plotted against the GOES class. Flare sizes range from $\sim 1.3 \times 10^9$ cm to 3.8×10^9 cm. The results reveal a weak inverse relationship, where stronger flares (higher GOES class) are associated with slightly smaller-scale structures. While larger flares can occur across a range of GOES classes, the most compact events are concentrated in the higher flux range (Fig. 1b).

3.1.3 Flare size vs. timescale

Fig. 2a examines the correlation between flare size (L) and flare duration (τ_{flare}). A moderate

positive trend is observed: flares with larger spatial dimensions tend to last longer, supporting reconnection-based scaling laws such as $\tau_{flare} \propto \frac{L}{V_{in}}$. This suggests that in larger coronal structures, the reconnection process operates over extended timescales, likely due to slower inflow or extended energy release regions (Fig. 2a).

3.1.4 Reconnection rate vs. GOES class

Fig. 2b presents the distribution of the magnetic reconnection rate (M_A) versus GOES class. The reconnection rates, calculated from inflow velocity and Alfvén velocity, lie within the range (10^{-4} to 10^{-3}) (Fig. 2a). A slight downward trend is evident, indicating that higher GOES-class flares tend to occur with lower normalized reconnection rates. This suggests that the intense energy output of strong flares may not necessarily stem from faster reconnection, but from larger magnetic flux density or more efficient energy conversion in smaller volumes. All reconnection rates fall within one order of magnitude of the theoretical limit predicted by the Petschek model, affirming the fast reconnection regime observed in the solar corona.

3.2 Solar activity and atmospheric/drought variability

Time series data for 2014 demonstrate that solar activity indices such as the Wolf Sunspot Number (WSN) and Sunspot Number (SSN) exhibited moderate variability, with WSN ranging between 80 and 120, and SSN between 100 and 140. As shown in Figure 4, atmospheric indices NAO and AO displayed significant seasonal dynamics. NAO declined from +0.8 in February to -0.97 in June, followed by sharp oscillations from -1.68 in August

to +2.0 in December. Similarly, AO showed a drop from +1.21 in March to -1.13 in October.

Correlation analysis revealed a moderately strong positive correlation between WSN and NAO ($r = 0.63$ at zero lag; $r = 0.43$ at two-month lag), suggesting that solar variability may influence mid-latitude circulation patterns both immediately and with short delay. The SPI3 drought index, which showed a strong correlation with NAO ($r = 0.70$), mirrored this variability – indicating drought intensification from March to June, followed by a recovery phase toward the end of the year. Furthermore, a moderately strong correlation

between WSN and SPI3 ($r = 0.57$) supports the hypothesis that solar activity, directly or indirectly, modulates regional drought conditions.

In parallel, the Hydrothermal Coefficient (HTC) showed a strong negative correlation with AO ($r = -0.75$), and AO itself correlated positively with SSN ($r = 0.51$), suggesting a solar-mediated influence on Arctic atmospheric patterns. Additionally, a strong negative correlation between SSN and HTC ($r = -0.66$) was observed, reinforcing the link between increased solar activity and suppressed precipitation in the mid-latitude continental region.

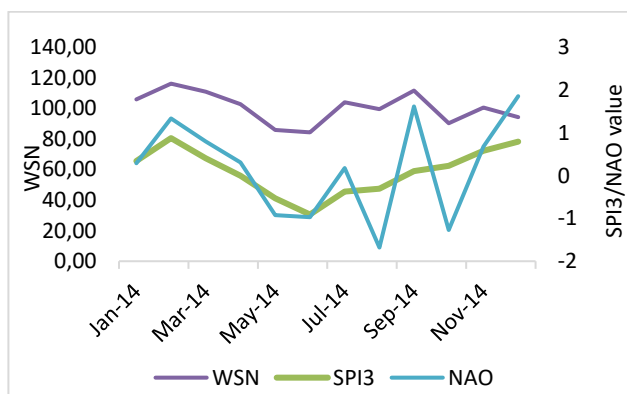


Figure 3 – Time variation of: WSN, SPI3, NAO

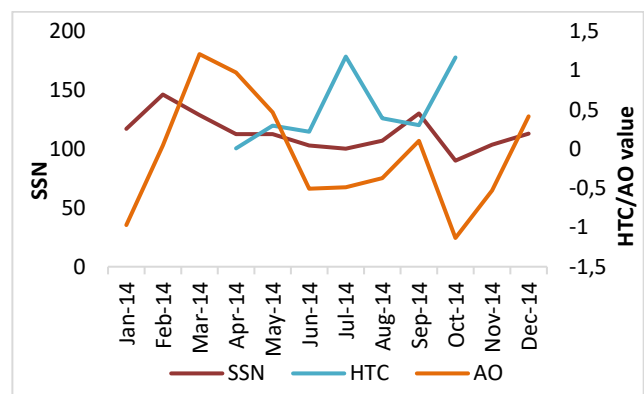


Figure 4 – Time variation of: SSN, HTC, AO

Figures 3 and 4 illustrate the temporal evolution of solar activity, atmospheric circulation indices, and drought indicators. Throughout 2014, the Wolf Sunspot Number (WSN) fluctuated between 80 and 120. The North Atlantic Oscillation (NAO) index declined steadily from February to June, reaching -0.97, and showed sharp variability during the summer, ranging from -1.68 in August to +2.0 in September and December. The SPI3 drought index, which exhibits a strong correlation with NAO ($r = 0.70$), indicated progressive drought intensification from March to June, followed by a trend toward wetter conditions by the end of the year.

Correlation analysis revealed a consistent and moderately strong positive relationship between WSN and NAO, with a maximum correlation coefficient of $r = 0.63$ at zero lag, decreasing to $r = 0.43$ with a two-month lag. Additionally, a moderately strong positive correlation between WSN and SPI3 was identified ($r = 0.57$), suggesting a potential solar influence on short-term hydrometeorological variability.

As shown in Figure 4, sunspot numbers (SSN) ranged between 100 and 140. The Arctic Oscillation (AO) index displayed significant seasonal variability, increasing from +1.21 in March to a minimum of -1.13 in October. The Hydrothermal Coefficient (HTC), which is strongly negatively correlated with AO ($r = -0.75$), showed persistently dry conditions from April to October. Correlation analysis revealed a moderately strong positive relationship between SSN and AO ($r = 0.51$) within a one-month lag. Furthermore, a strong negative correlation between SSN and HTC ($r = -0.66$) was established, indicating that elevated solar activity may be associated with increased meteorological drought conditions in mid-latitudes.

4 Conclusion

This study provides a comprehensive investigation into the solar-terrestrial connection by integrating detailed physical analysis of solar flare dynamics with regional atmospheric and

hydrometeorological responses. From the solar physics perspective, we estimated the physical parameters of 12 X- and M-class solar flares observed between January and December 2014, focusing on energy release rates and reconnection dynamics. The calculated reconnection rates ranged from 10^{-4} to 10^{-3} , and exhibited an inverse relationship with GOES flare class. These results are consistent with the theoretical predictions of the Petschek reconnection model, supporting the validity of magnetic reconnection as the dominant mechanism behind flare energy release. The energy output, derived from multi-wavelength observations, provides an important physical basis for quantifying solar forcing in Earth's upper atmosphere.

On the meteorological side, the findings highlight a coherent and statistically significant link between solar activity and large-scale atmospheric oscillations. A moderately strong correlation between WSN and NAO ($r = 0.63$ at zero lag; $r = 0.43$ at a two-month lag) suggests both immediate and delayed influences of solar variability – likely mediated through UV-induced stratospheric heating and subsequent modulation of planetary wave dynamics. These oscillatory responses appear to cascade into regional hydrometeorological effects, as evidenced by a strong positive correlation between NAO and SPI3 ($r = 0.70$), indicating that the positive phase of NAO is associated with

increased precipitation and reduced short-term drought in Northern Kazakhstan.

Importantly, the study also identifies a moderately strong direct relationship between solar activity and SPI3 ($r = 0.57$), further reinforcing the hypothesis that solar variability – particularly flarerelated energetic events – can influence regional drought regimes. A significant negative correlation between sunspot numbers and the Hydrothermal Coefficient (HTC) ($r = -0.66$) in mid-latitudes suggests that enhanced solar activity may correspond to drier conditions. This is further supported by a chain of correlations involving Arctic Oscillation (AO), where solar activity and AO exhibit a positive correlation ($r = 0.51$), and AO and HTC are strongly negatively correlated ($r = -0.75$). These results collectively point to a multi-step coupling mechanism, whereby solar magnetic activity modulates high-latitude atmospheric circulation (e.g., AO), which in turn affects surfacelevel climate indicators such as drought severity.

Acknowledgements. The research was funded by the Science Committee of the Ministry of Science and Higher Education of the Republic of Kazakhstan (Grant No. AP25796409 – “Risk assessment of atmospheric droughts and development of an early warning system for Northern Kazakhstan based on machine learning”).

References

1. Petschek H. E. Magnetic field annihilation. In *Physics of solar flares*, edited by W. N. Hess. NASA SP-50. Washington, DC, USA: NASA, 1964. –P. 425–439.
2. Parker E. N. Sweet's mechanism for merging magnetic fields in conducting fluids // *Journal of Geophysical Research*. –1957. –Vol. 62. –P. 509–520. <https://doi.org/10.1029/jz062i004p00509>
3. Parker E. N. The solar flare phenomenon and theory of reconnection and annihilation of magnetic fields // *Astrophysical Journal Supplement Series*. –1963. –Vol. 8. –P. 177–211.
4. Sweet P. A. *Electromagnetic phenomena in cosmical physics*. Cambridge: Cambridge University Press, 1958.
5. Schwabe S. Die Sonne // *Astronomical Notes*. –1843. –Vol. 20, No. 17. <https://doi.org/10.1002/asna.18430201706>
6. Wolf J. R. Mittheilungen über die Sonnenflecken // *Vierteljahrsschrift der Naturforschenden Gesellschaft in Zürich*. –1856. –Vol. 1. –P. 151–161. (In German)
7. Pol M., Binyamin J. Impact of climate change and variability on wheat and corn production in Buenos Aires, Argentina // *American Journal of Climate Change*. –2014. –Vol. 3, No. 2. –P. 145–152. <https://doi.org/10.4236/ajcc.2014.32013>
8. Liu Xiaokang, et al. Holocene solar activity imprint on centennial- to multidecadal-scale hydroclimatic oscillations in arid Central Asia // *Journal of Geophysical Research: Atmospheres*. –2019. –Vol. 124, No. 5. –P. 2562–2573. <https://doi.org/10.1029/2018jd029699>
9. Bojariu R., et al. Cryosphere–atmosphere interaction related to variability and change of Northern Hemisphere annular mode // *Annals of the New York Academy of Sciences*. –2008. –Vol. 1146, No. 1. –P. 50–59. <https://doi.org/10.1196/annals.1446.018>
10. Sawadogo Y., Koala S., and Zerbo J. L. Rainfall and temperature variations over Burkina Faso: Possible influence of geomagnetic activity, solar activity and associated energies from 1975 to 2020 // *Atmospheric and Climate Sciences*. –2022. –Vol. 12, No. 4. –P. 603–612. <https://doi.org/10.4236/acs.2022.124034>
11. Owoicho A. M., and Okeke F. N. Seasonal variability of rainfall and its decadal anomaly over Nigeria: Possible role of solar and geomagnetic activities // *International Journal of Advanced Engineering Research and Science*. –2018. –Vol. 5, No. 9. –P. 325–335. <https://doi.org/10.22161/ijaers.5.9.39>

- 12.Kodera K. Solar influence on the Indian Ocean monsoon through dynamical processes // *Geophysical Research Letters*. – 2004. –Vol. 31, No. 24. <https://doi.org/10.1029/2004gl020928>
- 13.Mathpal M. C., Pande B., and Pande S. Dependence of rainfall on solar activity features // *Journal of Mountain Research*. – 2019. –Vol. 14, No. 1. <https://doi.org/10.51220/jmr.v14i1.18>
- 14.Mohamed M. A., and El-Mahdy M. E.-S. Impact of sunspot activity on the rainfall patterns over Eastern Africa: A case study of Sudan and South Sudan // *Journal of Water and Climate Change*. –2021. –Vol. 12, No. 5. –P. 2104–2124. <https://doi.org/10.2166/wcc.2021.312>
- 15.Maghrabi A. H., Alamoudi H. A., and Alruhaili A. S. Investigation of a possible link between solar activity and climate change in Saudi Arabia: Rainfall patterns // *Atmospheric and Climate Sciences*. –2023. –Vol. 13. –P. 478–490. <https://doi.org/10.4236/acs.2023.134027>
- 16.Zharkova V., et al. Heartbeat of the Sun from principal component analysis and prediction of solar activity on a millennium timescale // *Scientific Reports*. –2015. –Vol. 5. –P. 15689. <https://doi.org/10.1038/srep15689>
- 17.Nagashima K. Statistical study of the reconnection rate in solar flares observed with Yohkoh SXT // *Astrophysical Journal*. – 2006. –Vol. 647. –P. 654.
- 18.Sarsembayeva A., Odsuren M., Belisarova F., Sarsembay A., Maftunzada S. A. L. Detecting the Sun's active region using image processing techniques // *Physical Sciences and Technology*. –2021. –Vol. 8(3–4). –P. 48–53. <https://doi.org/10.26577/phst.2021.v8.i2.07>
- 19.Sarsembayeva A., Belisarova F., Odsuren M., Sarsembay A. February 25, 2014 solar flare data analysis in SunPy // *Physical Sciences and Technology*. –2020. –Vol. 7(3–4). –P. 21–25. <https://doi.org/10.26577/phst.2020.v7.i2.03>
- 20.Sarsembayeva A., Belisarova F., Odsuren M., Sarsembay A. A new Java-based application in solar physics // *Physical Sciences and Technology*. –2019. –Vol. 6(3–4). –P. 22–27. <https://doi.org/10.26577/phst-2019-2-p3>
- 21.Garcia H. A. Forecasting methods for occurrence and magnitude of proton storms with solar hard X rays // *Space Weather*. – 2004. –Vol. 2. –P. S06003. <https://doi.org/10.1029/2003SW000035>
- 22.Isobe H., Takasaki H., and Shibata K. Measurement of the energy release rate and the reconnection rate in solar flares // *Astrophysical Journal*. –2005. –Vol. 632. –P. 1184. <https://doi.org/10.1086/444490>
- 23.Vicente-Serrano S. M., Beguería S., and López-Moreno J. I. A multiscalar drought index sensitive to global warming: The standardized precipitation evapotranspiration index // *Journal of Climate*. –2010. –Vol. 23. –P. 1696–1718. <https://doi.org/10.1175/2009JCLI2909.1>
- 24.Selyaninov G. T. Proiskhozhdenie i dinamika zasukh [Origin and dynamics of droughts]. In *Zasukh v SSSR, ikh proiskhozhdenie, povtoryaemost' i vliyaniye na urozhai*, edited by A. Rudenko, –P. 36–44. Leningrad: Gidrometeoizdat, 1958. (In Russian)
- 25.NOAA National Centers for Environmental Information. North Atlantic Oscillation (NAO) index page. <https://www.ncei.noaa.gov/access/monitoring/nao/> (accessed April 21, 2025).
- 26.NOAA Physical Sciences Laboratory. Monthly AO index (Arctic Oscillation). <https://psl.noaa.gov/data/timeseries/month/AO/> (accessed April 21, 2025).

Information about the author:

Sarsembayeva Aiganym, PhD is an Associate professor at the Department of Theoretical and Nuclear Physics, Al-Farabi Kazakh National University (Almaty, Kazakhstan), e-mail: sarsembayeva.a@kaznu.kz;

Ryssaliyeva Laura Sergeevna is a Senior researcher at the Department of Meteorology and Hydrology, Al-Farabi Kazakh National University (Almaty, Kazakhstan), e-mail: ryssaliyeva.laura@kaznu.kz;

Belissarova Farida, PhD is an Associate professor at the Department of Theoretical and Nuclear Physics, Al-Farabi Kazakh National University (Almaty, Kazakhstan), e-mail: farida.belisarova@kaznu.kz;

Sarsembay Akmaral, M.Sc., is a CSI «Kyzylorda Regional Educational Center (Methodological Office)» of the Department of Education of Kyzylorda Region, (Kyzylorda, Kazakhstan), e-mail: akmaral_sarsembay@mail.ru.